Amide conjugates of the DO3A-*N*-(α-amino)propionate ligand: leads for stable, high relaxivity contrast agents for MRI?

Miguel F. Ferreira,[a] André F. Martins[b,c] Catarina I.O. Martins,[b] Paula M. Ferreira,[a] Éva Tóth,[c] Tiago B. Rodrigues,[d,e] Daniel Calle,[f] Sebastian Cerdan,[f] Pilar López-Larrubia,[f] José A. Martins[a*] and Carlos F.G.C. Geralde[b,g,h]

[a] Centro de Química, Campus de Gualtar, Universidade do Minho, 4710-057 Braga, Portugal

[b]Center of Neurosciences and Cell Biology, University of Coimbra, Largo Marquês de Pombal, Coimbra, Portugal

[c]Centre de Biophysique Moléculaire UPR 4301, CNRS, Rue Charles Sadron, 45071 Orléans, France

[d]Cancer Research UK, Cambridge Research Institute, Li Ka Shing Centre, Cambridge CB2 0RE, United Kingdom

[e]Department of Biochemistry, University of Cambridge, Cambridge CB2 1GA, United Kingdom

[f]Instituto de Investigaciones Biomédicas "Alberto Sols", CSIC-UAM, Madrid, Spain

[g]Department of Life Sciences, Faculty of Science and Technology, University of Coimbra, P.O. Box 3046, 3001-401 Coimbra, Portugal.

[h]Centro de Química de Coimbra, Rua Larga, University of Coimbra, 3004-535 Coimbra, Portugal

Corresponding author: José A. Martins, Centro de Química, Campus de Gualtar, Universidade do Minho, 4710-057 Braga, Portugal.

Keywords: DO3A-*N*-(α-amido)propionate chelators; Gd(DO3A-*N*-(α-benzoylamido)propionate) chelate; fast water exchange; pH stability; safety; *in vivo* MRI

Abstract

A novel synthetic methodology for preparing amide conjugates of the DO3A-*N*-(α-amino)propionate chelator is described, using the synthesis of the DO3A-*N*-(α-benzoylamido)propionate chelator as an illustrative example. The model Gd(DO3A-*N*-(α-benzoylamido)propionate) chelate displays accelerated water exchange, stability in a wide pH range and inertness towards transmetallation by Zn^{2+}. The Gd(DO3A-*N*-(α-benzoylamido)propionate) complex is mainly excreted via the kidneys, producing a significant increase of the kidney medulla/cortex enhancement ratio in MR images of Wistar rats, reflecting probably its increased hydrophobicity compared to Gd(DTPA). The results presented suggest that Gd(DO3A-*N*-(α-amido)propionate) chelates can be valuable leads for preparing potentially safe high relaxivity MRI contrast agents.

Introduction

Since its introduction around 30 years ago, MRI has evolved into the leading imaging modality both in the clinics and in biomedical sciences (1). Incremental developments in instrumentation, particularly the use of increasingly higher magnetic fields, and the use of contrast agents (CAs), have driven MRI to the forefront of medical imaging (2). Gd^{3+} chelates are the most useful CAs for MRI due to the high paramagnetism (7 unpaired electrons) and long electronic relaxation times of the Gd^{3+} ion (3). To ensure safety, Gd^{3+} ions are used as complexes with poly(aminocarboxylate) ligands, which prevents the inherent toxicity of the free metal ion and modulates its unfavorable pharmacokinetic behaviour. The efficacy of a CA is measured by its relaxivity (r_1, r_2)- the enhancement of the relaxation rate of the water protons brought about by a 1 mM concentration of Gd^{3+} (4,5). Increasing detection sensitivity, by maximizing relaxivity, has been the driving force in the development of new CAs (6). Nonetheless, the high relaxivities predicted theoretically haven't yet been achieved in spite of the tremendous efforts and developments in the field (7). The main approaches to enhance detection sensitivity involve optimizing the relaxivity of individual chelates, clustering a high number of (high relaxivity) chelates into (bio)macromolecular carriers or self-assembly of monomeric chelates into supramolecular structures, and directing chelate constructs to the sites of interest by attaching targeting moieties recognized specifically by cellular receptors (6,8). All these approaches require chemical modification of the basic chelator structure in order to introduce "handles" for chemical functionalization.

A few years ago, the discovery of severe toxicity associated with repeated CA MRI in individuals suffering from kidney function impairment cast doubt about the safety of MRI CAs (9,10). This condition, named Nefrogenic Systemic Fibrosis (NSF), owing to generalized formation of fibrotic (scarring) plates in the skin and internal organs, was correlated with the use of Gd^{3+} chelates of DTPA *bis*-amide chelators (11). Release of Gd^{3+} ions *in vivo*, owing to insufficient kinetic and thermodynamic stability of the Gd(DTPA-*bis*-amide) chelates, seems the most likely reason for CA toxicity (12,13). Importantly, only a few cases have been associated with macrocyclic CAs of the DOTA family, all in patients suffering from kidney disease (13-15). The much higher kinetic and thermodynamic stability of the macrocyclic DOTA-type CAs precludes release of Gd^{3+} ions *in vivo*. The adoption of stricter guidelines concerning the use of Gd^{3+}-based CA has drastically reduced the number of NSF cases reported (16).

Nonetheless, safety, associated to chelate stability, rather than high relaxivity (high detection sensitivity), is becoming the new paradigm in CA MRI, which favours the use of macrocyclic, DOTA-type CAs. There are several CAs of this type approved for clinical use in Europe, most of which are extracellular CAs. Gd(HPDO3A) (Prohance®) has become one of the CAs of choice in the clinical setting (17). Improving the performance of DOTA-type CAs (targeting, multimerization, responsiveness, etc.) requires chemical elaboration of the basic DOTA scaffold to allow conjugation to (bio)molecules. Endowing DOTA chelators with conjugability without compromising stability is a core problem in CA research. In fact, the most convenient route for chemical functionalization of the DOTA skeleton, differentiating an acetate arm for amide coupling, reduces the thermodynamic and kinetic inertness of Gd(DOTA-monoamide)-type chelates (18). Furthermore, neutral Gd(DOTA-monoamide)-type chelates display much slower water exchange, limiting the relaxivities potentially achievable by chelates displaying optimized rotational correlation times (τ_R). Introducing pendant functional groups on the ethylenediamine bridges on the DOTA skeleton is an effective, although costly solution (19). It is preferable from the synthetic point of view to elaborate the (pre-formed) available *cyclen* skeleton than starting chelator synthesis from scratch. We have recently reported the synthesis of a new chelator, DO3A-*N*-(α-amino)propionate (**L_2**, Scheme 1) and the relaxometric characterization of its Gd^{3+} complex. The α-amino substituted propionate arm presumably imposes steric compression around the water binding site on the complex, resulting in an accelerated water exchange rate k_{ex} (20). In the same year, Botta and co-workers reported a bifunctional chelator, DOTAMAP-En, and an amide conjugate, DOTAMAP-En-C18, bearing a propionamide arm. Even higher water exchange rates were demonstrated for the Gd(DOTAMAP-En) and for the Gd(DOTAMAP-En-C18) chelates, presumably also owing to steric compression (21). The k_{ex} value for the Gd(DO3A-*N*-(α-amino)propionate) **(**Gd**L_2)** chelate is of the same order of magnitude as that reported for its (unsubstituted) propionate analogue Gd(DOTA-*N*-propionate)- in the range considered ideal for attaining high relativities at intermediate/high field (18,20,22). Moreover, the Gd**L_2** complex is stable in the pH range 2-10 and inert towards transmetallation with Zn^{2+}. The pendant available amine group is ideal for conjugation through a variety of ligation chemistries.

We have recently reported the preparation of a cysteinyl conjugate of the DO3A-*N*-(α-amino)propionate chelator using an advanced protected intermediate on route to the DO3A-*N*-(α-amino)propionate chelator, as originally proposed (23). However, an important issue remains to be addressed: *what is the effect of amide conjugation on the stability and water exchange rate of Gd(DO3A-N-(α-amido)propionate) chelates?* In this manuscript we describe a novel expeditious methodology for the synthesis of amide conjugates of the DO3A-*N*-(α-amino)propionate chelator. The relaxometric characterization and *in vivo* MRI evaluation of a model amide chelate, Gd(DO3A-*N*-(α-benzoylamido)propionate) (Gd**L$_1$**), is reported.

Results and Discussion

Synthesis

Allying stability to conjugability is an important requisite for developing metal chelates into imaging and/or therapeutic agents. We have proposed before that the pendant amine group on the α-aminopropionate arm on the DO3A-*N*-(α-amino)propionate chelator is an ideal handle for conjugation to (bio)molecules (20). There are literature precedents for the direct conjugation of functionalised (pre-formed) chelates (24). However, solubility issues and difficult manipulations and purifications can be avoided, especially with radio-labelled metal chelates, by labelling fully deprotected conjugates. A cysteinyl conjugate of the DO3A-*N*-(α-amino)propionate was recently described by us using the "conventional approach": amide coupling of a *S*,*N*-protected cysteinyl block to a protected advanced intermediate followed by deprotection (23). In this work we disclose a new expeditious strategy for the synthesis of amide conjugates of the DO3A-*N*-(α-amino)propionate scaffold (Scheme 1).

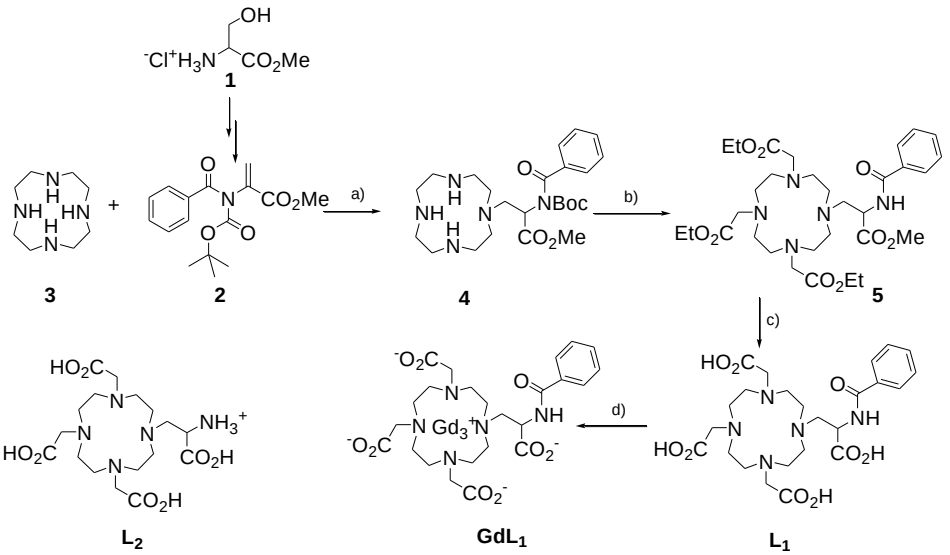

L_2 - DO3A-N-(α-amino)propionate
Ferreira et al *Chem. Comm.*, 2009, 42, 6475

L_1- DO3A-*N*-(α–benzoylamido)propionate

Scheme 1. Synthetic sequence for the DO3A-*N*-(α-benzoylamido)propionate ligand and its Gd^{3+} chelate. a) K_2CO_3, MeCN; b) i. TFA/DCM, ii. K_2CO_3/ethyl bromoacetate, MeCN; c) i. Dowex 1X2100-OH- resin, ii. Elution with hydrochloric acid 0.1 M; d) $GdCl_3.xH_2O$.

Introducing a pre-formed Boc-dehydroamide (Ph, Boc)-Δ-AlaOMe **2** into the cyclen scaffold *via* Michael addition is the key step in this reaction sequence. Building up on our previous experience on the synthesis of bifunctional chelator $\mathbf{L_2}$ we envisaged that (Boc, amide)-dehydroalanines of type **2** could fulfil electronic and steric requirements to perform well as electrophiles in Michael addition to cyclen. (Boc, amide)-dehydroalanines of type **2** can be readily prepared in two steps from serine methyl ester hydrochloride **1** and stored at room temperature for extended periods (25). Michael addition of block (**2**) to cyclen **3** proceeded smoothly in acetonitrile, using K_2CO_3 as base, in 2-3 hours. An excess of cyclen, 1.5 eq., was used in order to bias the statistical mixture towards the monoalkylated product **4**. Removing the Boc group at the monoalkylated intermediate **4** stage could avert retro-elimination during the next alkylation step. In fact, one pot treatment of **4** with TFA, followed by alkylation with ethyl bromoacetate in the presence of a large excess of K_2CO_3 produced the fully alkylated amide **5** in moderate yield without evidence of retro-elimination. One step deprotection of the fully alkylated pro-chelator **5** with ion-exchange resin Dowex 1X2 OH^- followed by elution with hydrochloric acid yielded the fully deprotected DO3A-*N*-(α-benzoylamido)propionate chelator $\mathbf{L_1}$ in overall (non-optimised yield) of 16% over 3 steps. Introducing the pre-formed amide onto the cyclen scaffold early on the synthesis is an unusual strategy. This conjugation strategy avoids orthogonal protection schemes and multistep deprotection for obtaining the final conjugates. Moreover, synthesising the amide separately and performing the "coupling" early on the synthesis avoids difficult purifications and reduces the risk of contamination of the final conjugates with bi-products of (carbodiimide-based) coupling reagents (23). This approach is general, applicable to Boc-dehydroamides of type **2** lacking acid sensitive moieties/protecting groups and basic sites susceptible to alkylation on the amide moiety.

Solution NMR and relaxometric studies

As discussed above, the aim of this work is to ascertain if Gd^{3+} chelates of amide conjugates of the DO3A-*N*-(α-amino)propionate metal chelator retain the high stability, inertness and fast water exchange of its parent Gd$\mathbf{L_2}$ complex. The soluble, low molecular weight Gd$\mathbf{L_1}$ complex (Scheme 1) was selected as a model system in order to avoid solubility and self-assembly complicating issues.

^{1}H NMR spectra at 600 MHz of $\mathbf{L_1}$ complexes (Ln^{3+}= La, Sm and Eu) at 298 K and neutral pH were found to contain very broad resonances for the macrocyclic and pendant arm methylene protons, indicating the presence of an internal isomerisation process at intermediate exchange on the NMR time scale (26). The temperature dependence of the ^{1}H spectrum of the $\mathbf{EuL_1}$ complex studied at lower frequency (300 MHz) provides direct proof of this process. In fact, the spectrum at 280 K contains more than fifty sharp resonances, corresponding to slow exchange between two isomers of C_1 symmetry, which are broadened at higher temperature (Figure 1SI: Supporting Information). The large positive shifts of the two sets of four resonances observed in the low temperature spectrum result from the four axial protons of the Eu^{3+} complex in the square antiprismatic (SA) and twisted square antiprismatic (TSA) conformations with a 60:40 population ratio, while the parent Eu$\mathbf{L_2}$ complex in the same conditions indicates a 98% predominance of the SA conformation (20). Thus, the derivatization of the amine function of $\mathbf{L_2}$ favours the TSA form.

The water exchange rate, k_{ex}^{298}, for the Gd$\mathbf{L_1}$ complex was determined from variable-temperature ^{17}O NMR studies (Figure 1 a and b). Additionally, the magnetic field dependence of the longitudinal water proton relaxivities (r_1) was measured by ^{1}H nuclear magnetic relaxation dispersion (NMRD) at 298 and 310 K (Figure 1c) with the objective of determining the parameters that describe water exchange and rotational dynamics for the Gd$\mathbf{L_1}$ complex.

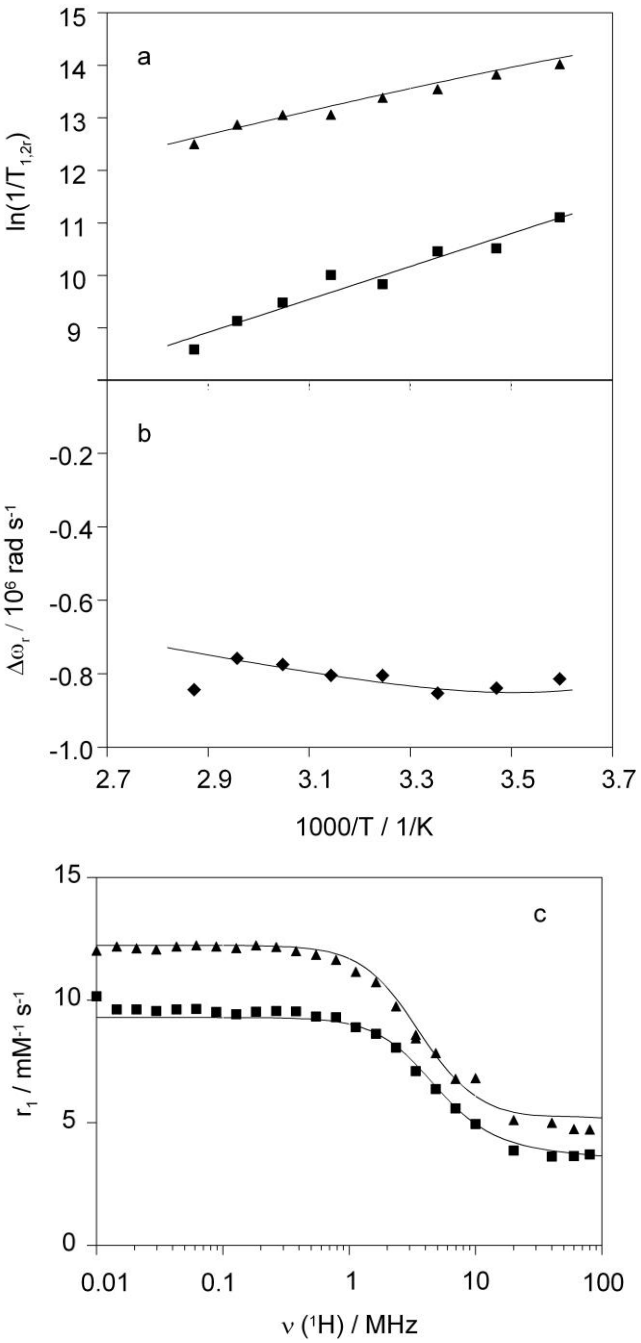

Figure 1. Temperature dependence of the (a) reduced transverse and longitudinal ^{17}O relaxation rates $1/T_{2r}$ and $1/T_{1r}$, and (b) chemical shifts $\Delta\omega_r$; B = 9.4 T ($\ln(1/T_{1r})$, (■), ($\ln(1/T_{2r})$, (▲)), and (c) NMRD profiles (298 K (▲) and 310 K (■) for the Gd(DO3A-*N*-(α-benzoylamido)propionate) complex.

The Solomon-Blombergen-Morgan theory was used for analyzing simultaneously the experimental ^1H NMRD data, as well as the ^{17}O NMR reduced longitudinal ($1/T_{1r}$) and transverse ($1/T_{2r}$) relaxation rates and chemical shifts ($\Delta\omega_r$) (5). In the analysis, the following parameters have been fitted: rate (k_{ex}^{298}), activation enthalpy ($\Delta H^{\ddagger}$) and activation entropy ($\Delta S^{\ddagger}$) of the water exchange, the rotational correlation time (τ_{RH}^{298}) and its activation energy (E_R), the electron spin relaxation parameters (τ_V^{298}, Δ^2 and E_V)

and the scalar coupling constant (A/ħ). The diffusion constant and its activation energy have been fixed to D_{GdH}^{298} = 26 x 10^{-10} m^2s^{-1} and E_{DGdH}^{298} = 22 kJ/mol, respectively. The Gd-water proton distance was fixed to r_{GdH} = 3.1Å, and the distance of closest approach between the Gd^{3+} ion and the outer sphere protons to Gd_H = 3.6 Å (22,27).
The parameters obtained from the simultaneous fitting of the data are shown on Table 1, and the corresponding fitted curves are shown in Figure 1.

Table 1. Best fit parameters obtained for the Gd(DO3A-*N*-(α-benzoylamido)propionate) chelate from the simultaneous fitting of the NMRD data, ^{17}O NMR longitudinal ($1/T_{1r}$) and transverse ($1/T_{2r}$) relaxation rates and chemical shifts ($\Delta\omega_r$).

Parameters	**GdL_1**[a]	**GdL_2**[b]	**Gd(DOTA)**[c]
$q(H_2O)$	1	1	1
$\Delta H^{\ddagger}$[J/K/mol]	17±1.1	19.1	54.5
$\Delta S^{\ddagger}$[kJ/mol]	-40±6	-35	+65
k_{ex}^{298} [10^7 s^{-1}]	5.14 ± 0.4	4	0.46
E_R [kJ/mol]	26.2±1.1	17	20
τ_{RH}^{298}[ps]	182±10	71	100
E_V [kJ/mol]	4.8±0.5	1	8.6
τ_V^{298} [ps]	7.2±1.5	11	0.65
Δ^2 [10^{20} s^{-2}]	0.5±0.06	0.25	0.12[d]
A/ħ [10^6 rad/s]	-3.13±0.4	-3.6	-4.0

[a]Parameters underlined have been fixed. [b] From ref.(20). [c] From ref. (27). [d] From ref. (28)

In the fitting, one inner sphere water molecule was assumed in analogy with the parent Gd**L_2** complex (20). This assumption was confirmed by the value obtained for the parameter *A/ħ*, characteristic of *q = 1* complexes of the DOTA family. The rate constant for water exchange for the Gd**L_1** complex (k_{ex}^{298} = (5.14 ±0.4) x 10^7 s^{-1}) is of the same order of magnitude as that reported for its parent Gd**L_2** complex (k_{ex}^{298} = (4±0.4) x 10^7 s^{-1}) (20) and for the unsubstituted Gd(DOTA-*N*-propionate) complex (k_{ex}^{298} = 6.1 x 10^7 s^{-1}) (18). Moreover, k_{ex} is around one order of magnitude higher than that reported for Gd(DOTA)(27). This result confirms our working hypothesis, that Gd^{3+} chelates of amide conjugates of the DO3A-*N*-(α-amino)propionate chelator retain the fast water exchange displayed by its parent Gd**L_2** complex. This is an important result, suggesting that amide conjugates displaying an optimized rotational correlation time, τ_R, could attain high relaxivities at intermediate fields.

The value for the rotational correlation time obtained from the ^{1}H longitudinal relaxation rates (τ_{RH}^{298} = 182 ps) is characteristic of low molecular weight chelates, indicating that the complex does not self-assemble in the concentration range studied. At high magnetic fields, the relaxivity is dominated by fast rotation in solution, as demonstrated by its temperature dependence (Figure 2SI).

Besides thermodynamic stability, the kinetic stability of the Gd^{3+} complexes is of paramount importance for meaningful biological applications. The *in vivo* dissociation of a GdL complex depends on the exchange reactions taking place in the blood plasma, such as with the most abundant bidentate anions like carbonate (~26 mM), L-lactate (~2.3 mM), or phosphate (~1.1 mM) (29, 30). The time dependence of the relative water proton paramagnetic relaxation rate $R_{1p}(t)/R_{1p}(0)$ for the Gd**L$_1$** complex in 10 mM phosphate buffer is shown in Figure 2. Addition of 6.7 equiv. of phosphate to a 1.5 mM solution of the complex causes a fast decrease in R_{1p} of 10%, indicating a weak interaction of the complex with phosphate, possibly replacing the inner-sphere water molecule by adduct formation in a monodentate binding mode (31). Larger (~25% decreasing) effects of phosphate on the relaxivity of Gd^{3+} complexes with two inner-sphere water molecules have been observed (32).

Metal exchange reactions with endogenous metal ions, the most abundant of which in blood plasma (besides Ca^{2+} and Mg^{2+}) is Zn^{2+} (29, 30), have been proposed to be the most likely mechanisms for Gd^{3+} leakage (33, 34). This can occur via the direct attack of the endogenous metal on GdL, or via proton-assisted dissociation of GdL, followed by recombination of the ligand with the attacking metal ion (35-37). Kinetic studies carried out close to physiological pH using much higher cationic concentrations than the free concentrations expected in plasma, led to the general conclusion that the dissociation of DTPA-like linear complexes occurs mainly via direct transmetallation, while the much slower dissociation of DOTA-like macrocyclic chelates uses mainly proton-assisted pathways (35-37).

The kinetic inertness of the Gd**L$_1$** complex was evaluated using the simple transmetallation assay developed by Muller and co-workers (38). Complex transmetallation by Zn^{2+} was studied in phosphate-buffer (10 mM, pH 7.1) (Figure 2). Replacement of Gd^{3+} by Zn^{2+} in the initial complex generates a time-dependent decrease of the paramagnetic contribution to the water proton spin-lattice relaxation rate (R_{1p}) due to precipitation of $GdPO_4$.

The time evolution of the relative water proton paramagnetic relaxation rate $R_{1p}(t)/R_{1p}(0)$ for the Gd**L**$_1$ complex in phosphate buffer, in the absence and in the presence of Zn^{2+} (Figure 2) fulfils the accepted empirical criteria for kinetic and thermodynamic stability (38). Although the Zn^{2+} concentrations used in this empirical assay are several orders of magnitude higher than its free or exchangeable concentrations in plasma (30), the results provide a fast initial screening between inert and labile Gd^{3+} complexes. Furthermore, the independence of the paramagnetic relaxation rates for the Gd**L**$_1$ complex from the solution pH (Figure 3SI) confirms that the complex is stable in the pH range 2-11.

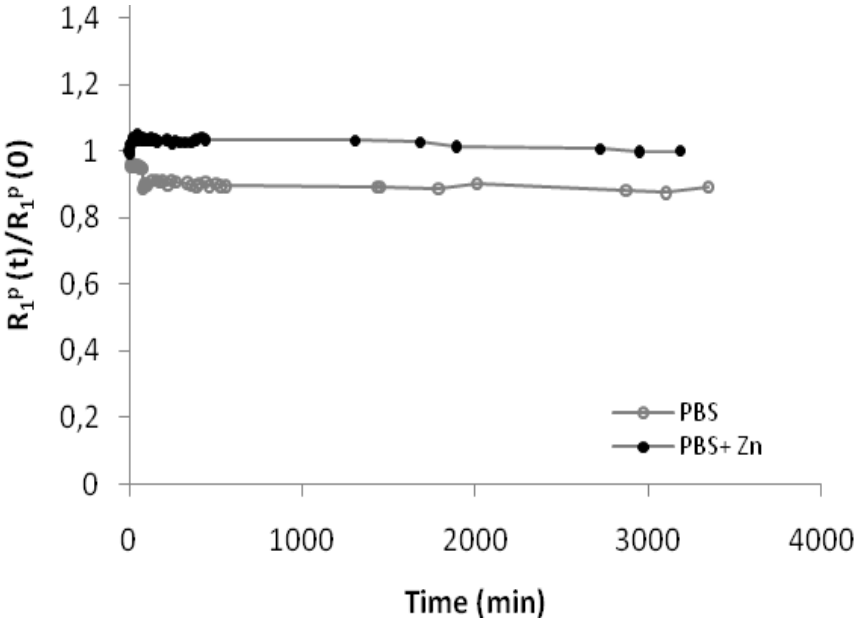

Figure 2. Evolution of the relative water proton paramagnetic relaxation rate $R_{1p}(t)/R_{1p}(0)$ (20 MHz, pH 7.1, 298 K) versus time for a 1.5 mM solution of Gd(DO3A-*N*-(α-benzoylamido)propionate complex in phosphate buffer (10 mM, pH 7.1) (○) and in phosphate buffer containing an equimolar amount of Zn^{2+} ions (●).

The interaction of the Gd**L1** complex with human serum albumin (HSA) was studied by relaxometric titration (Figure 4SI). A very weak binding was detected, which is not likely to affect the pharmacokinetic behaviour of the complex *in vivo*.

MRI Studies

Comparative MRI studies have been performed at 7.0 Tesla in male Wistar rats with Gd**L$_1$** and Gd(DTPA). The Gd**L$_1$** contrast agent was well tolerated by the animals at the dose used. No gross side effects were observed during the injection, immediately or several days after the experiment. During experiments, rats body temperature remained stable and no alteration on the body functions was observed. Overall, Gd**L$_1$** seemed to be harmless to the animals. Nevertheless, a more detailed study would be required to further assess its toxicology.

Figure 3 shows a representative series of T_1-weighted spin-echo axial images of the Dynamic Contrast Enhanced (DCE) experiments obtained before and after injection of the Gd**L$_1$** complex (dose 0.1 mmol Gd/kg body weight) and, for comparison purposes, Gd(DTPA) at the same dose. In the pre-injection image, kidney structures (cortex, inner and outer medulla) and adjacent tissues were dark due to the particular inversion delay chosen. After bolus injection in the vascular system, a strong signal enhancement was observed in the kidneys for the two CAs, as a result of the T_1 shortening. A slighter signal enhancement was observed in liver and muscle for both CAs. As can be seen, both complexes follow mainly renal elimination by glomerular filtration with a very small hepatobiliary contribution to excretion.

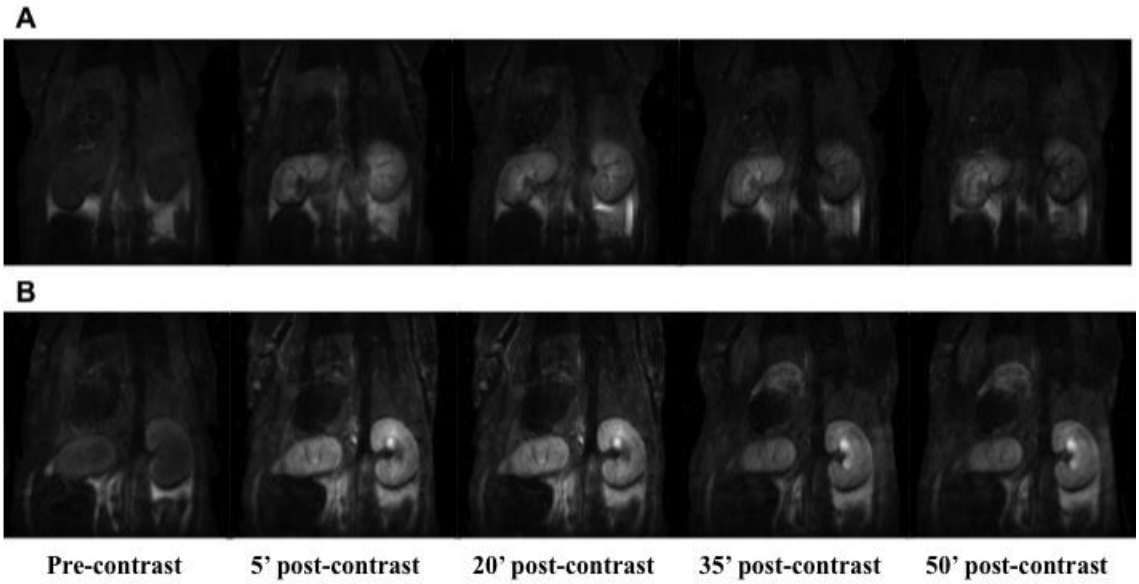

Figure 3. Representative coronal T_1-weighted spin echo MR images of a Wistar rat before and after injection of the contrast agents (**A**) Gd**L**$_1$ (dose 0.1 mmol kg^{-1} BW), (**B**) Gd**(DTPA)** (dose 0.1 mmol kg^{-1} BW).

The features of the data in Figure 3 are better understood as illustrated in Figure 4, which shows their quantitative analysis. Each time point corresponds to the average intensity within ROIs placed on the different organs. In order to compare the results for all the animals under study (n = 4), the data were normalized by calculating the mean relative enhancement of each ROI. The scattering in the time course curves of the average relative enhancement of the ROIs was caused by animal respiratory motion. Muscle and liver enhancement is comparably low with both complexes. The relative enhancement obtained with Gd(DTPA) increased almost immediately after intravenous injection from 0 up to about 250% in the kidney medulla and 200% in the kidney cortex, followed by a steady decrease to values around 120% and 80%, respectively, after 50 minutes. The time course of the average relative enhancement after injection of Gd(DTPA) (Figure 4A) is in good agreement with the literature for Gd(DTPA) (39,40) or other low molecular weight Gd-based contrast agents (41-45).

The renal pharmacokinetic behavior of **GdL_1** is significantly different from that observed for Gd(DTPA). Kidney cortex enhancement build-up is slower than for Gd(DTPA), reaching a maximum of about 100% after 10 minutes post injection, followed by a steady decrease to a value (~80%) comparable to that reached by Gd(DTPA) after 50 minutes.

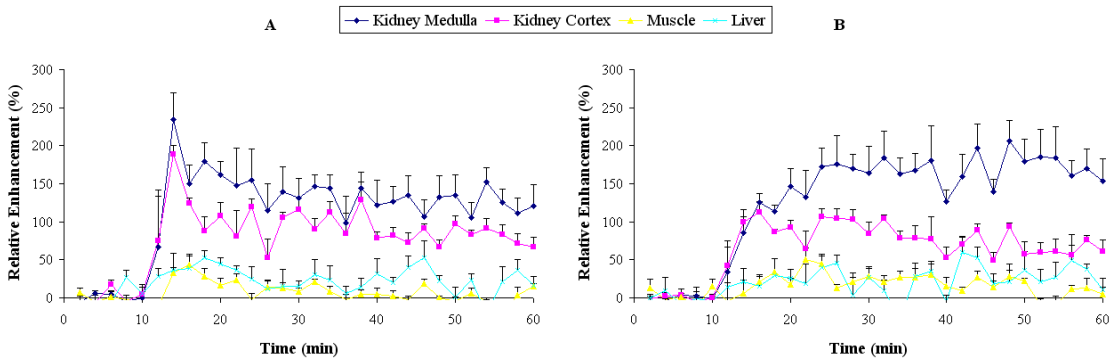

Figure 4. Time course of signal intensity, relative to the initial value (up to 50 min post-injection) of several regions of interest during dynamic contrast enhancement MRI experiments in rats with (**A**) Gd(DTPA) (0.1 mmol kg^{-1} BW) and (**B**) **GdL_1** (0.1 mmol kg^{-1} BW). The time courses are data for mean values of four animals and the corresponding standard error.

However, the main difference between **GdL_1** and Gd(DTPA) regards kidney medulla enhancement. While for Gd(DTPA) there is a sharp increase just after injection, followed by a steady decrease, for the **GdL_1** complex a saturation-like kinetic behaviour is observable.

After 50 minutes, a significantly higher enhancement of the kidney medulla is attained with the **GdL_1** complex comparing to Gd(DTPA) (200% *vs* 120%). At the same dose, the **GdL_1** complex resulted in a considerably lower initial signal enhancement than Gd(DTPA) at both the cortex and medulla, which is not in agreement with their in vitro relaxivities, which are comparable. As a consequence of the disparate pharmacokinetics, the ratio of medulla/cortex enhancement increases significantly for the **GdL_1** complex over the duration of the experiment, while it is approximately constant for the Gd(DTPA) complex.

The pharmacokinetic behaviour in rats of the Gd(DOTA) complex regarding kidney excretion is similar to that displayed by the Gd(DTPA) complex (41): a sharp enhancement of kidney medulla and cortex after injection followed by a steady decrease with the enhancement ratio medulla/cortex approximately constant over the experiment duration. This suggests that, although charge effects (-2 for the Gd(DTPA) complex and -1 for the Gd**L_1** complex) cannot be ruled out, the observed difference of pharmacokinetic behaviour is likely due to the higher hydrophobicity of the Gd**L_1** complex comparing to the Gd(DTPA) complex.

It has been shown previously that the in vitro and in vivo relaxivities of Gd-based CAs can be significantly different, as the latter are affected by tissue structure and physiology (39,46). Gd(DTPA) was found to display relaxivities considerably lower in rat kidney cortex or medulla comparing to the values measured in saline solution or in other tissues. This effect is related to CA compartmentalization in the kidney (47,48). The quantitative determination of the in vivo relaxivity of a CA requires knowledge of its local concentration. In some cases, CA concentration has been obtained from independent measurements. These studies, however, are not without difficulties, since they often induce significant perturbations to the tissues, by studying intact excised tissues (49), making measurements post-mortem (47), or ensuring a constant infusion of the CA in order to establish a steady state concentration (48).

Lacking such experiments, estimation of the relative in vivo relaxivities would require to measure the effective T_1 values on different ROIs, to assume a linear dependence of signal enhancement with the local CA concentration, and the unacceptable assumption of similar pharmacokinetics for Gd(DTPA) and **GdL_1** (43). Therefore, this quantitative pharmacokinetic study, which is beyond the scope of the present work, is not feasible in the present case.

One can safely conclude from the present study that the pharmacokinetic behaviour of both CAs is different, especially in the kidney medulla at later stages of excretion.

.

Conclusions

In this manuscript we describe the synthesis of the benzoylamide conjugate of the DO3A-*N*-(α-amino)propionate chelator as an illustrative example of a new, general methodology for the expeditious preparation of amide conjugates. The Gd(DO3A-*N*-(α-benzoylamido)propionate) chelate retains the fast water exchange and stability of its parent Gd(DO3A-*N*-(α-amino)propionate) complex.

DCE-MRI studies in rats revealed that the Gd(DO3A-*N*-(α-benzoylamido)propionate) chelate is mainly excreted via the kidneys. A significant increase of the kidney medulla/kidney cortex enhancement ratio is produced by the contrast agent after 50 minutes, reflecting probably its increased hydrophobicity compared to Gd(DTPA).

The results presented here suggest that Gd(DO3A-*N*-(α-amido)propionate) chelates are valuable leads for preparing potentially safe high relaxivity MRI CAs. In fact, Gd(DO3A-*N*-(α-amido)propionate) chelates with optimized water exchange features, when bound to suitable carriers, are likely to originate high relaxivities at intermediate fields by virtue of the simultaneous optimisation of k_{ex} and τ_R (23). The high relaxivities of such imaging platforms allied to chelate stability and safety could find many uses in biomedical and pre-clinical diagnostic MRI applications.

Experimental

Materials and Methods

Chemicals were purchased from Sigma-Aldrich and used without further purification. Solvents used were of reagent grade and purified by usual methods. Cyclen was purchase from CheMatech. Reactions were monitored by TLC on Kieselgel 60 F254 (Merck) on aluminium support. Detection was by examination under UV light (254 nm) and by adsorption of iodine vapour. Flash chromatography was performed on Kieselgel 60 (Merck, mesh 230–400). The relevant fractions from flash chromatography were pooled and concentrated under reduced pressure, T < 313 K. Ion exchange chromatography was performed on Dowex1X2100-OH^- resin (Sigma Aldrich).

The resin was purchase as the Cl^- form and converted to the OH^- form by the standard procedure. ^1H and ^{13}C NMR spectra (assigned by 2D DQF-COSY and HMQC techniques) were run on a Varian Unity Plus 300 NMR spectrometer, operating at 299.938 MHz and 75.428 MHz, for ^1H and ^{13}C, respectively. Chemical shifts (δ) are given in ppm relative to the $CDCl_3$ solvent (^1H, δ 7.27; ^{13}C, δ 77.36) as internal standard. For ^1H and ^{13}C spectra recorded in D_2O, chemical shifts (δ) are given in ppm relative to TSP as internal reference (1H, δ 0.0) and *tert*-butanol as external reference (^{13}C, CH_3 δ 30.29). The Gd^{3+} concentration of the complex preparation used for *in vivo* MRI was determined by inductively coupled plasma optical emission spectrometry (ICP-OES).

(2-(*N*-*t*-butoxycarbonyl)benzamido)-methoxycarbonylethyl-1,4,7,10-tetrazacyclododecane - monoalkylated cyclen (4): K_2CO_3 (4.07 g, 29.5 mmol) was added to a solution of cyclen (1.27 g, 7.37 mmol) in MeCN (50 ml). To this solution was added (Ph, Boc)-Δ-AlaOMe **2** (1.5 g, 4.91 mmol). The suspension was stirred vigorously at room temperature for 3 hrs. The suspension was filtered and the filtrate was evaporated under reduced pressure. The residue was purified by flash chromatography (100% CH_2Cl_2 → CH_2Cl_2/EtOH/NH_3/H_2O (70:30:5:5)) to afford compound **4** as a viscous light yellow oil (1.34 g, 59.1%). ^1H NMR (300 MHz, $CDCl_3$): δ = 1.47 (s, 9H, Boc), 2.50-2.90 (m, 16H, N(*CH*$_2$)2N), 3.01 (dd, *J*= 14.1 and 6 Hz, 1 H, N*CH*$_a$H$_b$CH), 3.49 (dd, *J*= 14.4 and 5.1 Hz, 1 H, N*CH*$_a$*H*$_b$CH), 3.76 (s, 3H, OMe), 5.25 (t, *J*= 6 and 5.1 Hz, 1H, NCH$_a$H$_b$*CH*), 7.30-7.70 (5H, m, Ar). ^{13}C NMR (75.4 MHz, $CDCl_3$): δ= 27.27 (C(*C*H$_3$)$_3$), 44.77 (*C*H$_2$), 45.83 (*C*H$_2$), 46.70 (*C*H$_2$), 51.27 (*C*H$_2$), 52.51 (O*C*H$_3$), 55.61 (N*C*H$_2$CH), 56.08 (*C*H), 83.88 (*C*(CH$_3$)$_3$), 127.87 (Ar), 127.96 (Ar), 131.27 (Ar), 137.02 (Ar), 152.72 (N*C*(O)O), 170.57 (C(O)Ar), 172.62 (*C*(O)OCH$_3$). HRMS (ESI): m/z: cacd for $C_{24}H_{39}N_5O_5$: 478.3029, found: 478.3024.

2-benzamido-methoxycarbonylethyl-4,7,10-tris-(ethoxycarbonylmethyl)-1,4,7,10-tetrazacyclododecane- tetraalkylated cyclen (5)- :A solution of monoalkylated cyclen **4** (1.30 g, 2.72 mmol) in a solution of trifluoroacetic acid in dichlorometane (60%, 25 ml) was stirred overnight at room temperature. The solvent was evaporated at reduced pressure and the residue was redissolved in dichloromethane. This procedure was repeated several times to give a light yellow thick oil.

^{1}H NMR spectroscopy ($CDCl_3$) revealed the disappearance of the signals assigned to the *Boc* groups in the precursor compound **4**. Quantitative deprotection was assumed. To a solution of Boc-deprotected compound **4** (2.72 mmol, assuming quantitative deprotection) in MeCN (40 ml) was added K_2CO_3 (4.51 g, 32.6 mmol). The suspension was vigorously stirred for 30 minutes at room temperature before adding ethyl bromoacetate (1.06 ml, 9.52 mmol). The suspension was further stirred at room temperature for 2.5 hrs. The suspended solid was removed by filtration, the filtrate was evaporated under reduce pressure and the residue was purified by flash chromatography (100% CH_2Cl_2 → CH_2Cl_2/EtOH (1:1)) to afford compound **5** (0.632 g, 37%) as a white foam. ^{1}H NMR (300 MHz, $CDCl_3$): δ= 1.22 (m, 9 H, CH_2CH_3), 2.2-3.60 (broad, overlapped signals with a integration corresponding to, 24 H, NCH_2 and NCH_aH_bCH), 3.71 (s, 3H, C(O)OCH_3), 5.14 (m (br), 1H, NCH$_a$H$_b$*CH*), 7.44-8.03 (5H, m, Ar). ^{13}C NMR (75.4 MHz, $CDCl_3$): selected signals: 13.95 (CH_2CH_3), 48.74 (*CH*), 49.04 (CH_2), 50.38 (CH_2), 51.48 (CH_2), 52.59 (CH_2), 52.95 (OCH_3), 53.62 (CH_2CH), 53.62 (CH_2), 54.86 (CH_2), 54.96 (CH_2), 55.19 (CH_2), 55.37 (CH_2), 55.75 (CH_2), 56.18 (CH_2), 60.62 (CH_2), 60.94, 61.13, 61.21 (OCH_2), 127,83 (Ar), 128,12 (Ar), 128,41 (Ar), 131,53 (Ar), 131,84 (Ar), 132.62 (Ar), 167.79 (C(O)Ar), 170.29 (2X C(O)OCH_2), 170.52 (C(O)OCH_3), 170.91 (C(O)OCH_2). HRMS (ESI): m/z: cacd for $C_{31}H_{49}N_5O_9$: 636.3609, found: 636.3590.

2-benzamido-carboxyethyl-4,7,10-tris-(carboxymethyl)-1,4,7,10-tetrazacyclododecane - DO3A-*N*-(α-benzoylamido)propionate metal chelator (L_1): Compound **5** (0.566 g, 0.89 mmol) was dissolved in a mixture made up of 20 ml of water and 20 ml of ethanol. The solution was adjusted to pH ~ 10-11 by adding small portions of Dowex 1X2-100-OH^- resin. The suspension was kept under stirring at room temperature for 2 hours. The wet resin was transferred into a chromatography column, washed with water (~50 ml) and eluted with 0.1 M hydrochloric acid. The relevant fractions, identified by TLC (ethanol water 1/1, revelation with iodine vapor) were pooled, concentrated at room temperature and further dried under vacuum to afford the final deprotected compound, in the hydrochloride form, as a light yellow solid (**6**) (0.276 g, 71.2%). ^{1}H NMR (300 MHz, $CDCl_3$): δ= 2.9-3.6 (broad, overlapped signals with a integration corresponding to, 18 H, N(CH_2)$_2$N and NCH$_a$H$_b$*CH*), 3.81 (broad, overlapped signals with a integration corresponding to, 6 H, NCH_2), 4.80 (m (br), ^{1}H, *CH*), 7.53-7.88 (5H, m, Ar). ^{13}C NMR (75.4 MHz, $CDCl_3$): selected signals: 43.02

(*CH*$_2$), 48.11 (*CH*$_2$), 48.93 (*CH*$_2$), 49.03 (*CH*$_2$), 49.78 (*CH*$_2$), 51.39 (*CH*$_2$), 51.71 (*CH*), 51.91 (*CH*$_2$), 54.53 (*CH*$_2$), 56.08 (*CH*$_2$), 56.77 (2x *CH*$_2$), 127,46 (2x Ar), 129,04 (2x Ar), 132,60 (Ar), 133.32 (Ar), 170.20 (C(O)), 177.17 (*C*(O)Ar). HRMS (ESI): m/z: cacd for $C_{24}H_{36}N_5O_9$: 538.2513, found: 538.2508.

^{1}H and ^{17}O NMR and ^{1}H NMRD experiments

Sample preparation

To an aqueous solution of the ligand (pH = 5.0) was added drop-wise an aqueous solution of the corresponding $LnCl_3.xH_2O$ lanthanide in a 1:1 mole ratio. The solution was stirred at room temperature over 1 hour while keeping its pH at around 5.7 by adding aqueous KOH. The solution was keft stirring at room temperature overnight. The solution was concentrated under reduced pressure to afford off white solids. The solutions for NMR measurements were obtained by dissolution of the appropriate amounts of solid complexes in D_2O (V = 1 ml) to obtain 20 mM concentrations. Proton 1D spectra of the solutions of the paramagnetic (Sm^{3+} and Eu^{3+}) and diamagnetic (La^{3+}) complexes were obtained at 298 K on a Varian VNMRS 600 (14.09 T, 600.14 MHz) NMR spectrometer and the temperature dependence of the ^{1}H NMR spectra of the Eu^{3+} complex on a Varian Unity Plus 300 NMR spectrometer.

The solutions of the Gd**L$_1$** complex for ^{17}O NMR and ^{1}H NMRD experiments were prepared by mixing equimolar amounts of $GdCl_3$ and ligand. A slight excess (5%) of ligand was used. The solution was adjusted to pH ~5.8 with aqueous NaOH and was allowed to react for 24 hours at room temperature. The absence of free metal was checked in each sample by testing with xylenol orange (50,51). HPLC analysis (RP C18 silica, isocratic elution with acetonitrile/water (70:30), detection at λ= 265 nm) of an aqueous solutiom of the Gd(DO3A-*N*-(α-benzoylamido)propionate) complex (8 mM, pH 7.0) indicates that the complex is > 95 pure (Figure 5SI). The pH of the stock solution was adjusted by adding aqueous NaOH (0.1 mM). ^{17}O-enriched water (^{17}O: 11.4%) was added to the solutions for ^{17}O measurements to improve sensitivity. The final concentration of the complex solution was 17.56 mmol kg^{-1} at pH = 6.90. For the NMRD experiments a 5.00 mM solution of complex at pH 6.98 was used.

^{17}O NMR experiments

Variable-temperature ^{17}O NMR measurements were performed on a Bruker Avance-500 (11.7 T) spectrometer. A BVT-3000 temperature control unit was used to stabilize the temperature, measured by a substitution technique. The samples were sealed in glass spheres that fitted into 10 mm o.d. NMR tubes, to eliminate susceptibility corrections to the chemical shifts (41). Longitudinal relaxation rates ($1/T_1$) were obtained by the inversion recovery method, and transverse relaxation rates ($1/T_2$) by the Carr-Purcell-Meiboom-Gill spin-echo technique. As an external reference, acidified water of pH 3.4 was used.

NMRD measurements

The measurements were performed by using a Stelar Spinmaster FFC NMR relaxometer (0.01–20 MHz) equipped with a VTC90 temperature control unit. At higher fields, the ^{1}H relaxivity measurements were performed on a Bruker Electromagnet at the frequencies of 30 MHz, 40 MHz, 60 MHz and 80 MHz. In each case, the temperature was measured by a substitution technique. Variable temperature measurements were performed at 25 and 37°C.

Relaxivity studies of pH dependence and Zn^{2+} transmetallation

The transmetallation reaction of Gd**L$_1$** with Zn^{2+} was studied by following the time dependent decrease of the water proton longitudinal relaxation rate, R_1, of a phosphate-buffered saline solution (PBS, pH 7.1, 10 mM) containing 1.5 mM of Gd**L$_1$** after adding an equimolar amount of $ZnCl_2$ while the sample was vigorously stirred (53). The water longitudinal relaxation rate was also measured as a function of time on the PBS buffered solution (pH 7.1, 10 mM) containing 2.5 mM Gd**L$_1$** (54). The pH dependence of the relaxivity of the Gd**L$_1$** solution was also measured. A Bruker Minispec mq20 (20 MHz, 298 K) relaxometer was used for all measurements.

MRI experiments

***In vivo* MRI studies.** The experimental protocols performed were approved by the appropriate institutional review committees and meet the guidelines of their responsible governmental agency.

The Magnetic Resonance Imaging (MRI) experiments were all performed on a Bruker Pharmascan platform (Bruker Medical Gmbh, Ettlingen, Germany) using a 7.0 T horizontal-bore superconducting magnet, equipped with a ^{1}H selective 60 mm birdcage resonator and a Bruker gradient insert with 90 mm diameter (maximum intensity 360 mT/m). Data were acquired using a Hewlett-Packard console running Paravision software (Bruker Medical Gmbh, Ettlingen, Germany) under a LINUX environment.

All MRI examinations were carried out on male Wistar rats (n = 4, 250-260 g body weight) anaesthetized initially by inhalation in an induction box with O_2 (1 l/min) containing 3 % isoflurane, and maintained during the experiment using a face mask allowing free breathing and 1-2 % isoflurane on O_2. Animals were taped down into a holder, to minimize breathing-related motion, and were then placed in a heated probe, which maintained the core body temperature at 37 ± 0.5 °C, monitored by a rectal probe. The physiological state of the animal was monitored throughout the entire experiment by a Biotrig physiological monitor (Bruker Medical Gmbh, Ettlingen, Germany), using the respiratory rate and body temperature. 100 mM solutions of Gd(DO3A-*N*-(α-benzoylamido)propionate (Gd**L$_1$**) and Gd(DTPA) (Magnevist®, Schering, Berlin, Germany) were prepared in distilled water and the pH was adjusted to 7.2. The solutions were injected into the catheterized tail vein as a bolus in 20 s (0.1 mmol $Gd.kg^{-1}$ body weight) using an infusion pump (Panlab, Barcelona, Spain). Regional contrast agent uptake was assessed using Dynamic Contrast Enhanced (DCE) MRI. DCE MRI experiments were performed with series of T_1-weighted spin echo images sequentially acquired over 1 h, before and following the injection of the contrast agent 10 min after the beginning of the study. The acquisition parameters were: TR = 310 ms, TE = 10.58 ms, number of averages = 2, ten coronal slices, slice thickness = 2 mm, FOV = 5.0 x 5.0 cm, matrix = 256 x 256, 30 repetitions with a total acquision time of 119 s.

MRI data analysis. Data were analyzed with the public domain software Image J (http://rsbweb.nih.gov/ij/). With the aim of comparing the pharmacokinetics obtained from different animals, the data were normalized by calculating the percentage of relative, rather than absolute, enhancement:

$$RE = \frac{(I - I_0)}{I_0} \times 100$$

where I is the signal intensity at any given time after CA injection and I_0 is the intensity before injection.

The pharmacokinetic behaviour was analyzed by calculating the average enhancements within the different regions of interest (ROIs) placed on each one of the following regions: liver, kidney medulla, kidney cortex and muscle.

Acknowledgements

This work was financially supported by Fundação para a Ciência e a Tecnologia, Portugal: project PTDC/QUI/70063/2006, including a grant to C.I.O.M., grant SFRH/BD/63994/2009 to M.F.F. and grant SFRH/BD/46370/2008 to A.F.M. and Rede Nacional de RMN (REDE/1517/RMN/2005) for the acquisition of the Varian VNMRS 600 NMR spectrometer in Coimbra. T.B.R. was supported by a Marie Curie Fellowship (FP/-PEOPLE-2009-IEF 254380) and an EMBO Fellowship (ALTF 1145-2009). Financial support from La Ligue Contre le Cancer, France (E. T.), and from Ministerio de Ciencia e Innovación, Spain: projects SAF2011-23622 (S.C.) and CTQ2010-20960-C02-02 (P.L.-L.), and Comunidad de Madrid, Spain, project S2010/BMD-2349 (S.C. and P.L.-L). This work was carried out in the frame of the COST D38 Action "Metal Based Systems for Molecular Imaging" and COST TD1004.

Supplementary Information. Figure 1SI: ^{1}H NMR spectra (300 MHz) for the Eu**L$_1$** complex at different temperatures (280 K (7 ºC), 298 K (25 ºC), 313 K (40ºC) and 333 K (60 ºC) and neutral pH.

Figure 2SI: Temperature dependency of the water proton longitudinal paramagnetic relaxation rate R_{1p} (20 MHz, 25 ºC) for a Gd**L$_1$** solution (1.5 mM, pH 7.0).

Figure 3SI: pH dependency of the water proton longitudinal paramagnetic relaxation rate R_{1p} (20 MHz, 25 ºC) for a 1.5 mM solutiom of Gd**L$_1$**.

Figure 4SI: Concentration dependency of the water proton longitudinal paramagnetic relaxation rate R_{1p} (20 MHz, 25 ºC, pH = 7.1) for Gd**L$_1$** solutions in water (triangles) and in the presence of 4% (0.6 mM) HSA in water (circles) and in a phosphate buffer (PBS, 5 mM) (diamonds).

Figure 5SI: HPLC chromatogram (RP C18 silica, isocratic elution with acetonitrile/water (70:30), detection at λ = 265 nm) for a Gd**L$_1$** aqueous solution (8 mM, pH 7.0).

References

1. Runge VM, Gelblum DY. Future directions in magnetic resonance contrast media. Topics in magnetic resonance imaging : TMRI 1991;3(2):85-97.
2. Vlaardingerbroek MT, Boer, Jacques A. Magnetic Resonance Imaging: Theory and Practice. Berlin - Heidelberg: Springer; 2002.
3. Bonnet CS, Toth E. Towards highly efficient, intelligent and bimodal imaging probes: Novel approaches provided by lanthanide coordination chemistry. C R Chim 2010;13(6-7):700-714.
4. Caravan P, Ellison JJ, McMurry TJ, Lauffer RB. Gadolinium(III) chelates as MRI contrast agents: Structure, dynamics, and applications. Chem Rev 1999;99(9):2293-2352.
5. The Chemistry of Contrast Agents in Medical Magnetic Resonance Imaging. Merbach AE, Tóth É, Eds. Chichester: Wiley; 2001.
6. Aime S, Castelli DD, Crich SG, Gianolio E, Terreno E. Pushing the Sensitivity Envelope of Lanthanide-Based Magnetic Resonance Imaging (MRI) Contrast Agents for Molecular Imaging Applications. Accounts of Chemical Research 2009;42(7):822-831.
7. Caravan P, Farrar CT, Frullano L, Uppal R. Influence of molecular parameters and increasing magnetic field strength on relaxivity of gadolinium- and manganese-based T1 contrast agents. Contrast Media & Molecular Imaging 2009;4(2):89-100.
8. Archibald SJ. Macrocyclic coordination chemistry. Annual Reports Section "A" (Inorganic Chemistry) 2011;107:274-296.
9. Thomsen HS. Nephrogenic Systemic Fibrosis: History and Epidemiology. Radiologic clinics of North America 2009;47(5):827-831.
10. Weinreb JC, Abu-Alfa AK. Gadolinium-based contrast agents and nephrogenic systemic fibrosis: why did it happen and what have we learned? J Magn Reson Imaging 2009;30(6):1236-1239.
11. Hasebroock KM, Serkova NJ. Toxicity of MRI and CT contrast agents. Expert Opinion on Drug Metabolism & Toxicology 2009;5(4):403-416.
12. Port M, Idée J-M, Medina C, Robic C, Sabatou M, Corot C. Efficiency, thermodynamic and kinetic stability of marketed gadolinium chelates and their possible clinical consequences: a critical review. BioMetals 2008;21(4):469-490.
13. Morcos SK. Extracellular gadolinium contrast agents: Differences in stability. European Journal of Radiology 2008;66(2):175-179.
14. Manjunath V, Perazella MA. Imaging patients with kidney disease in the era of NSF: can it be done safely? Clin Nephrol 2011;75(4):279-285.
15. Elmholdt TR, Jørgensen B, Ramsing M, Pedersen M, Olesen AB. Two cases of nephrogenic systemic fibrosis after exposure to the macrocyclic compound gadobutrol. NDT Plus 2010;3(3):285-287.
16. Kanal E, Barkovich AJ, Bell C, Borgstede JP, Bradley WG, Froelich JW, Gilk T, Gimbel JR, Gosbee J, Kuhni-Kaminski E, Lester JW, Nyenhuis J, Parag Y, Schaefer DJ, Sebek-Scoumis EA, Weinreb J, Zaremba LA, Wilcox P, Lucey L, Sass N, Safety tABRPoM. ACR Guidance Document for Safe MR Practices: 2007. American Journal of Roentgenology 2007;188(6):1447-1474.
17. Runge VM, Gelblum DY, Jacobson S. Gd HP-DO3A—Experimental evaluation in brain and renal MR. Magnetic Resonance Imaging 1991;9(1):79-87.
18. Jaszberenyi Z, Sour A, Toth E, Benmelouka M, Merbach AE. Fine-tuning water exchange on Gd-III poly(amino carboxylates) by modulation of steric crowding. Dalton Trans 2005(16):2713-2719.

19. Vanasschen C, Bouslimani N, Thonon D, Desreux JF. Gadolinium DOTA Chelates Featuring Alkyne Groups Directly Grafted on the Tetraaza Macrocyclic Ring: Synthesis, Relaxation Properties, "Click" Reaction, and High-Relaxivity Micelles. Inorg Chem 2011;50(18):8946-8958.
20. Ferreira MF, Martins AF, Martins JA, Ferreira PM, Toth E, Geraldes C. Gd(DO3A-N-alpha-aminopropionate): a versatile and easily available synthon with optimized water exchange for the synthesis of high relaxivity, targeted MRI contrast agents. Chem Commun 2009(42):6475-6477.
21. Tei L, Gugliotta G, Baranyai Z, Botta M. A new bifunctional GdIII complex of enhanced efficacy for MR-molecular imaging applications. Dalton Trans 2009(44):9712-9714.
22. Dunand FA, Tóth É, Hollister R, Merbach AE. Lipari-Szabo approach as a tool for the analysis of macromolecular gadolinium(III)-based MRI contrast agents illustrated by the [Gd(EGTA-BA-(CH2)12)]n^{n+} polymer. Journal of Biological Inorganic Chemistry 2001;6(3):247-255.
23. Ferreira MF, Mousavi B, Ferreira PM, Martins CIO, Helm L, Martins JA, Geraldes CFGC. Gold nanoparticles functionalised with stable, fast water exchanging Gd^{3+} chelates as high relaxivity contrast agents for MRI. Dalton Trans 2012; 41(18):5472-5475.
24. André JP, Tóth É, Fischer H, Seelig A, Mäcke HR, Merbach AE. High Relaxivity for Monomeric Gd(DOTA)-Based MRI Contrast Agents, Thanks to Micellar Self-Organization. Chemistry – A European Journal 1999;5(10):2977-2983.
25. Ferreira PMT, Maia HLS, Monteiro LS, Sacramento J. High yielding synthesis of dehydroamino acid and dehydropeptide derivatives. J Chem Soc-Perkin Trans 1 1999(24):3697-3703.
26. Kálmán FK, Baranyai Z, Tóth I, Bányai I, Király R, Brücher E, Aime S, Sun X, Sherry AD, Kovács Z. Synthesis, Potentiometric, Kinetic, and NMR Studies of 1,4,7,10-Tetraazacyclododecane-1,7-bis(acetic acid)-4,10-bis(methylenephosphonic acid) (DO2A2P) and its Complexes with Ca(II), Cu(II), Zn(II) and Lanthanide(III) Ions. Inorg Chem 2008;47(9):3851-3862.
27. Powell DH, Dhubhghaill OMN, Pubanz D, Helm L, Lebedev YS, Schlaepfer W, Merbach AE. Structural and Dynamic Parameters Obtained from 17O NMR, EPR, and NMRD Studies of Monomeric and Dimeric Gd^{3+} Complexes of Interest in Magnetic Resonance Imaging: An Integrated and Theoretically Self-Consistent Approach1. J Am Chem Soc 1996;118(39):9333-9346.
28. Micskei K, Helm L, Brücher E, Merbach AE, 17O NMR study of water exchange on $[Gd(DTPA)(H_2O)]^{2-}$ and $[Gd(DOTA)(H_2O)]^{-}$ related to NMR imaging, Inorg Chem 1993; 32: 3844-3850.
29. Nicolaeva LS, Chircov, V.V., Dobrynina, Pastorova, V.E. Molecular-biological problems of drug design and mechanism of drug design - Investigation of the anticoagulant activity of several low-molecular-weight endogenous ligands of blood plasma by methods of computer simulation and universal biological assay. Pharm Chem J 2005; 39 (2) 57-63.
30. May P.M., Linder PW, Williams DR, Computer simulation of metal-ion equilibria in biofluids: models for the low-molecular-weight complex distribution of calcium (II), magnesium(II), manganese(II), iron(III), copper(II), zinc(II) and lead(II) ions in human blood plasma, J Chem Soc Dalton Trans 1977; 6: 588-595.

31. Burai L, Hietapelto V, Király R, Tóth É, Brücher E, Stability constants and proton relaxation effects of ternary complexes formed between Gd-DTPA, Gd-DTPA-BMA, Gd-DOAT and Gd-EDTA and citrate, phosphate and carbonate ions, Magn Reson Med 1997, 38: 146-150.
32. Silvério S, Torres S, Martins AF,Martins JÁ, André JP, Helm L, Prata MIM, Santos Ac, Geraldes CFGC, Lanthanide chelates of (bis)-hydroxymethyl-substituted DTTA with potential application as contrast agents in magnetic resonance imaging. Dalton Trans. 2009; 4656-4670.
33. Tweedle MF, Hagan JJ, Kumar K, Mantha S, Chang CA, Reaction of gadolinium chelates with endogenously available ions, Magn Reson Imaging 1991, 9: 409-415.
34. Rofsky NM, Sherry AD, Lenkinski RE. Nephrogenic Systemic Fibrosis: A Chemical Perspective. Radiology 2008;247(3):608-612.
35. Tóth É, Brücher E, Lazar I, Tóth I, Kinetics of Formation and Dissociation of Lanthanide(III)-DOTA Complexes, Inorg. Chem. 1994; 33 (18): 4070–4076.
36. Kumar K, Chang CA, Tweedle MF, Equilibrium and kinetic studies of lanthanide complexes of macrocyclic polyamino carboxylates, Inorg Chem 1993; 32: 587-593.
37. Brücher E, Kinetic stabilities of gadolinium(III) chelates used as MRI contrast agents, in Contrast Agents I. Magnetic Resonance Imaging, Krause W Ed, Topics in Current Chemistry, Springer Verlag-Berlin: Berlin, 2002; Vol 221, 104
38. Laurent S, Vander Elst L, Henoumont C, Muller RN. How to measure the transmetallation of a gadolinium complex. Contrast Media & Molecular Imaging 2010; 5(6): 305-308.
39. Raghunand N, Howison C, Sherry AD, Zhang S, Gillies RJ. Renal and systemic pH imaging by contrast-enhanced MRI. Magn Reson Med 2003; 49(2): 249-257.
40. Laurent D, Poirier K, Wasvary J, Rudin M. Effect of essential hypertension on kidney function as measured in rat by dynamic MRI. Magn Reson Med 2002; 47(1): 127-134.
41. Tweedle MF, Eaton SM, Eckelman WC, Gaughan GT, Hagan JJ, Wedeking PW, Yost FJ. Comparative chemical structure and pharmacokinetics of MRI contrast agents. Invest Radiol 1988; 23 Suppl 1: S236-239.
42. Harpur ES, Worah D, Hals PA, Holtz E, Furuhama K, Nomura H. Preclinical safety assessment and pharmacokinetics of gadodiamide injection, a new magnetic resonance imaging contrast agent. Invest Radiol 1993; 28 Suppl 1: S28-43.
43. Baumann D, Rudin M. Quantitative assessment of rat kidney function by measuring the clearance of the contrast agent Gd(DOTA) using dynamic MRI. Magn Reson Imaging 2000; 18(5): 587-595.
44. Livramento JB, Weidensteiner C, Prata MIM, Allegrini PR, Geraldes CFGC, Helm L, Kneuer R, Merbach AE, Santos AC, Schmidt P, Tóth É, First *in vivo* MRI assessment of a self-assembled metallostar compound endowed with a remarkable high field relaxivity, Contrast Media Mol. Imaging, 2006; 1: 30-39.
45. Sousa PL, Livramento JB, Helm L, Merbach AE, Même W, Doan B-T, Beloeil J-C, Prata MIM, Santos AC, Geraldes CFGC, Tóth É, *In vivo* MRI assessment of a novel Gd^{III}-based contrast agent designed for high magnetic field applications, Contrast Media Mol. Imaging, 2008; 3: 78-85.
46. Pickup S, Wood AK, Kundel HL. Gadodiamide T1 relaxivity in brain tissue in vivo is lower than in saline. Magn Reson Med 2005;53(1):35-40.

47. Shuter B, Tofts PS, Wang SC, Pope JM. The relaxivity of Gd-EOB-DTPA and Gd-DTPA in liver and kidney of the Wistar rat. Magn Reson Imaging 1996; 14(3): 243-253.
48. Pedersen M, Morkenborg J, Jensen FT, Stodkilde-Jorgensen H, Djurhuus JC, Frokiaer J. In vivo measurements of relaxivities in the rat kidney cortex. J Magn Reson Imaging 2000; 12(2): 289-296.
49. Gillis A, Gray M, Burstein D. Relaxivity and diffusion of gadolinium agents in cartilage. Magn Reson Med 2002; 48(6): 1068-1071.
50. Hovland R, Aasen AJ, Klaveness J. Preparation and in vitro evaluation of GdDOTA-$(BOM)_4$; a novel angiographic MRI contrast agent. Org & Biomol Chem 2003; 1(10): 1707-1710.
51. Barge A, Cravotto G, Gianolio E, Fedeli F. How to determine free Gd and free ligand in solution of Gd chelates. A technical note. Contrast Media & Molecular Imaging 2006; 1(5): 184-188.
52. Hugi AD, Helm L, Merbach AE. Water Exchange on Hexaaquavanadium(III): a Variable-Temperature and Variable-Pressure 17O-NMR Study at 1.4 and 4.7 Tesla. Helv Chim Acta 1985; 68(2): 508-521.
53. Laurent S, Elst LV, Copoix F, Muller RN. Stability of MRI paramagnetic contrast media - A proton relaxometric protocol for transmetallation assessment. Invest Radiol 2001; 36(2):115-122.
54. Laurent S, Elst LV, Vroman A, Muller RN. Synthesis and physicochemical characterization of new C-functionalized derivatives of the gadolinium(III) complex with 3,6,10-tris(carboxymethyl)-3,6,10-triazadodecanedioic acid (H(5)ttda) exhibiting fast water exchange potential paramagnetic reporters for molecular imaging. Helv Chim Acta 2007; 90(3): 562-573.

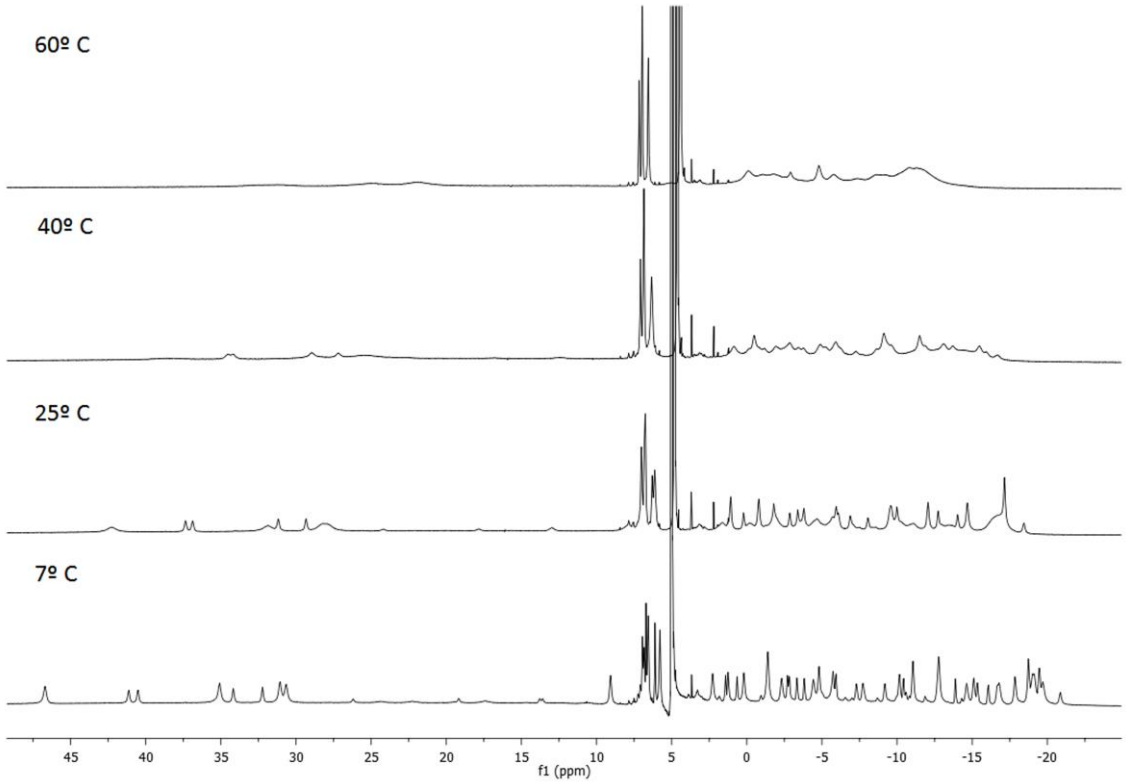

Figure 1SI. ^{1}H NMR spectra (300 MHz, D_2O) for the Eu(DO3A-*N*-(α-benzoylamido)propionate) complex at different temperatures.

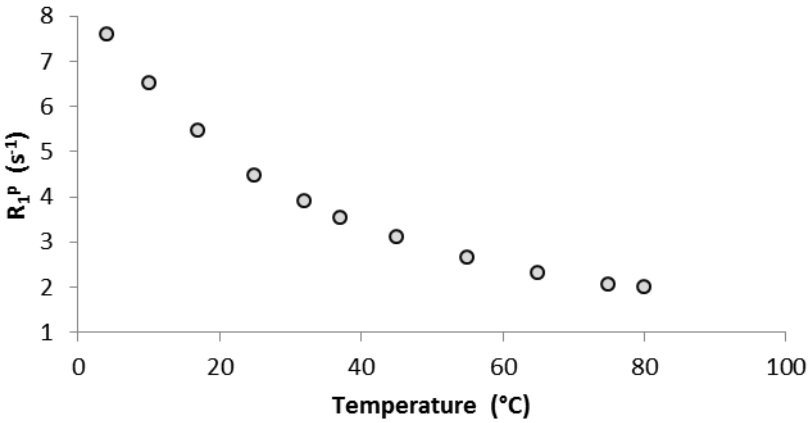

Figure 2SI. Temperature dependency of the water proton longitudinal paramagnetic relaxation rates R_{1p} (20 MHz, 25 ºC) for a 1.5 mM solution of Gd(DO3A-*N*-(α-benzoylamido)propionate.

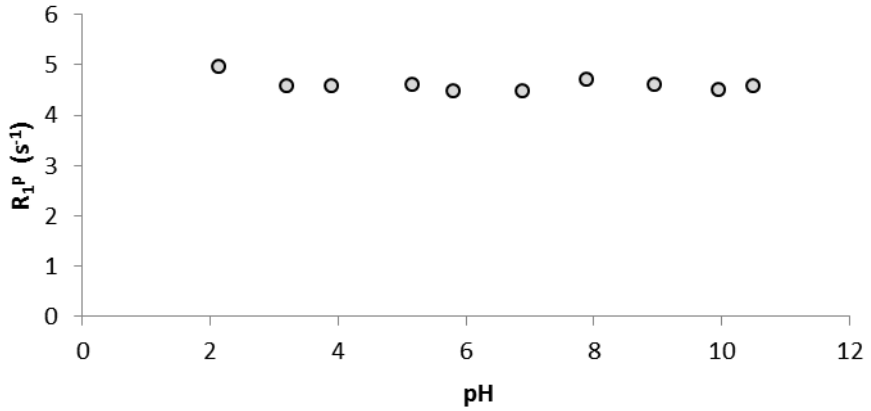

Figure 3SI. pH dependency of the water proton longitudinal paramagnetic relaxation rates R_{1p} (20 MHz, 25 ºC) for a 1.5 mM solution of Gd(DO3A-*N*-(α-benzoylamido)propionate.

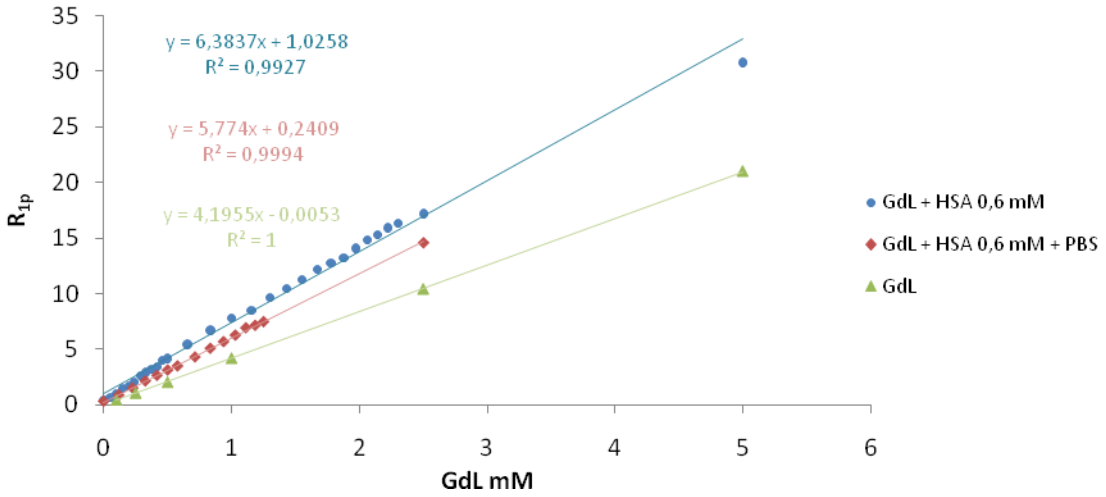

Figure 4SI. Dependency of the water proton longitudinal paramagnetic relaxation rates on the concentration of the Gd**L$_1$** complex in water (triangles), and in the presence of 4% (0.6 mM) HSA (circles) in water and in a phosphate buffer (PBS, 5 mM, pH = 7.1) (diamonds) (20 MHz, 298 K).

PKNO	TIME	AREA	MK	IDNO	CONC
1	1.782	128103	S		100
	TOTAL	128103			100

Figure 5SI: HPLC chromatogram (RP C18 silica, isocratic elution with acetonitrile/water (70:30), detection at λ = 265 nm) for a Gd**L$_1$** aqueous solution (8 mM, pH 7.0).

Equations used for the analysis of NMRD and ^{17}O NMR data

NMRD and ^{17}O NMR data have been analysed within the framework of the Solomon-Bloembergen-Morgan theory.

^{17}O NMR spectroscopy

From the measured ^{17}O NMR relaxation rates and angular frequencies of the paramagnetic solutions, $1/T_2$ and ω, and of the acidified water reference, $1/T_{2A}$ and ω_A, one can calculate the reduced relaxation rates and chemical shifts, $1/T_{2r}$ and $\Delta\omega_r$, which may be written as in Equations (A1)-(A2), where, $1/T_{2m}$ is the relaxation rate of the bound water and $\Delta\omega_m$ is the chemical shift difference between bound and bulk water, τ_m is the mean residence time or the inverse of the water exchange rate k_{ex} and P_m is the mole fraction of the bound water. [1, 2]

$$\frac{1}{T_{2\mathrm{r}}} = \frac{1}{P_m}\left[\frac{1}{T_2} - \frac{1}{T_{2\mathrm{A}}}\right] = \frac{1}{\tau_m}\frac{T_{2\mathrm{m}}^{-2} + \tau_m^{-1}T_{2\mathrm{m}-1} + \Delta\omega_m^2}{(\tau_m^{-1} + T_{2\mathrm{m}}^{-1})^2 + \Delta\omega_m^2} + \frac{1}{T_{2os}} \qquad \text{(A1)}$$

$$\Delta\omega_r = \frac{1}{P_m}(\omega - \omega_A) = \frac{\Delta\omega_m}{(1 + \tau_m T_{2\mathrm{m}}^{-1})^2 + \tau_m^2\Delta\omega_m^2} + \Delta\omega_{\mathrm{os}} \qquad \text{(A2)}$$

Previous studies have shown that outer sphere contributions to the ^{17}O relaxation rates are negligible. [3]

In equation (A2) the chemical shift of the bound water molecule, $\Delta\omega_m$, depends on the hyperfine interaction between the Gd^{III} electron spin and the ^{17}O nucleus and is directly proportional to the scalar coupling constant, $\frac{A}{\hbar}$, as expressed in Equation (A3). [4]

$$\Delta\omega_m = \frac{g_L\mu_B S(S+1)B}{3k_B T}\frac{A}{\hbar} \qquad \text{(A3)}$$

The isotopic Landé g factor is equal to 2.0 for the Gd^{III}, B represents the magnetic field, and k_B is the Boltzmann constant.

The outer-sphere contribution to the chemical shift is assumed to be linearly related to $\Delta\omega_m$ by a constant C_{os} [Equation (A4)]. [5]

$$\Delta\omega_{\mathrm{os}} = C_{\mathrm{os}}\Delta\omega_m \qquad \text{(A4)}$$

In the transverse relaxation, the scalar contribution, $1/T_{2sc}$, is the most important [Equation (A9)]. $1/\tau_{s1}$ is the sum of the exchange rate constant and the electron spin relaxation rate.

$$\frac{1}{T_{2\mathrm{m}}} = \frac{1}{T_{2\mathrm{sc}}} = \frac{S(S+1)}{3}\left(\frac{A}{\hbar}\right)^2 \tau_{s1} \qquad \text{(A5)}$$

$$\frac{1}{\tau_{\mathrm{s1}}} = \frac{1}{\tau_m} + \frac{1}{T_{1\mathrm{e}}} \qquad \text{(A6)}$$

The exchange rate is supposed to obey the Eyring equation. In equation (A7) $\Delta S^{\ddagger}$ and $\Delta H^{\ddagger}$ are the entropy and enthalpy of activation for the water exchange process, and k_{ex}^{298} is the exchange rate at 298.15 K.

$$\frac{1}{\tau_m} = k_{\mathrm{ex}} = \frac{k_B T}{h}\exp\left\{\frac{\Delta S^{\ddagger}}{R} - \frac{\Delta H^{\ddagger}}{RT}\right\} = \frac{k_{\mathrm{ex}}^{298} T}{298.15}\exp\left\{\frac{\Delta H^{\ddagger}}{R}\left(\frac{1}{298.15} - \frac{1}{T}\right)\right\} \qquad \text{(A7)}$$

NMRD

The measured longitudinal proton relaxation rate, $R_1^{obs} = 1/T_1^{obs}$, is the sum of a paramagnetic and a diamagnetic contribution as expressed in Equation (A12), where r_1 is the proton relaxivity:

$$R_1^{obs} = R_1^d + R_1^p = R_1^d + \mathrm{r}_1[\,\mathrm{Gd}^{3+}\,] \qquad \text{(A8)}$$

The relaxivity can be divided into an inner and an outer sphere term as follows:

$$r_1 = r_{1\mathrm{is}} + r_{1\mathrm{os}} \qquad \text{(A9)}$$

The inner sphere term is given in Equation (A14), where q is the number of inner sphere water molecules. [6]

$$r_{1\mathrm{is}} = \frac{1}{1000} \times \frac{q}{55.55} \times \frac{1}{T_{1\mathrm{m}}^H + \tau_m} \qquad \text{(A10)}$$

The longitudinal relaxation rate of inner sphere protons, $1/T_{1m}^H$ is expressed by Equation (A11), where r_{GdH} is the effective distance between the electron charge and the ^{1}H nucleus, ω_I is the proton resonance frequency and ω_S is the Larmor frequency of the Gd^{III} electron spin.

$$\frac{1}{T_{1\mathrm{m}}^H} = \frac{2}{15}\left(\frac{\mu_0}{4\pi}\right)^2 \frac{\hbar^2 \gamma_I^2 \gamma_S^2}{r_{GdH}^6} S(S+1) \times \left[3\mathrm{J}(\omega_I;\tau_{d1}) + 7\mathrm{J}(\omega_S;\tau_{d2})\right] \qquad \text{(A11)}$$

$$\frac{1}{T_i} = \frac{1}{T_{i\mathrm{m}}} + \frac{1}{T_{i\mathrm{RI}}} + \frac{1}{T_{i\mathrm{e}}} \quad \text{for } i = 1,2 \qquad \text{(A12)}$$

where τ_{RH} is the rotational correlation time of the Gd-H_{water} vector.

The rotational correlation time, τ_{RH} is assumed to have simple exponential temperature dependence with an E_R activation energy as given in equation (A13).

(A13)

The outer-sphere contribution can be described by Equation (A14) where N_A is the Avogadro constant, and J_{os} is its associated spectral density function as given by Equation (A15). [8, 9]

$$r_{1\mathrm{os}} = \frac{32N_A\pi}{405}\left(\frac{\mu_0}{4\pi}\right)^2 \frac{\hbar^2\gamma_S^2\gamma_I^2}{a_{\mathrm{GdH}}D_{\mathrm{GdH}}} S(S+1)\left[3\mathrm{J}_{\mathrm{os}}(\omega_I, T_{1\mathrm{e}}) + 7\mathrm{J}_{\mathrm{os}}(\omega_S, T_{2\mathrm{e}})\right] \qquad \text{(A14)}$$

$$J_{\mathrm{os}}(\omega, T_{je}) = \mathrm{Re}\left[\frac{1+14\left(i\omega\omega_{GdH}+\frac{\tau_{\mathrm{GdH}}}{T_{je}}\right)^{1/2}}{1+\left(i\omega\omega_{GdH}+\frac{\tau_{\mathrm{GdH}}}{T_{je}}\right)^{1/2}+49\left(i\omega\omega_{GdH}+\frac{\tau_{\mathrm{GdH}}}{T_{je}}\right)+19\left(i\omega\omega_{GdH}+\frac{\tau_{\mathrm{GdH}}}{T_{je}}\right)^{3/2}}\right] \qquad \text{(A15)}$$

$j = 1,2$

The longitudinal and transverse electronic relaxation rates, $1/T_{1e}$ and $1/T_{2e}$ are expressed by Equation (A16)-(A17), where τ_v is the electronic correlation time for the modulation of the zero-field-splitting interaction, E_v the corresponding activation energy and Δ^2 is the mean square zero-field-splitting energy. We assumed a simple exponential dependence of τ_v versus $1/T$ as written in Equation (A18).

$$\left(\frac{1}{T_{1e}}\right)^{\mathrm{ZFS}} = \frac{1}{25}\Delta^2\tau_v\left\{4S(S+1)-3\right\}\left(\frac{1}{1+\omega_S^2\tau_v^2}+\frac{4}{1+4\omega_S^2\tau_v^2}\right) \qquad \text{(A16)}$$

$$\left(\frac{1}{T_{2e}}\right)^{\mathrm{ZFS}} = \Delta^2\tau_v\left(\frac{5.26}{1+0.372\omega_S^2\tau_v^2}+\frac{7.18}{1+1.24\omega_S\tau_v}\right) \qquad \text{(A17)}$$

$$\tau_v = \tau_v^{298}\exp\left[\frac{E_v}{R}\left(\frac{1}{T}-\frac{1}{298.15}\right)\right] \qquad \text{(A18)}$$

The diffusion coefficient for the diffusion of a water proton away from a Gd^{III} complex,

D_{GdH}, is assumed to obey an exponential law versus the inverse of the temperature, with an activation energy $E_{DGdH,}$ as given in Equation (A19). D_{GdH}^{298} is the diffusion coefficient at 298.15K.

$$D_{\mathrm{GdH}} = D_{\mathrm{GdH}}^{298}\exp\left\{\frac{E_{\mathrm{GdH}}}{R}\left(\frac{1}{298.15}-\frac{1}{T}\right)\right\} \qquad \text{(A19)}$$

References for Equations

[1] T. J. Swift, R. E. Connick, *J. Chem. Phys.* **1962**, 37, 307-320.

[2] J. R. Zimmermann, W. E. Brittain, *J. Phys. Chem.* **1957**, 61, 1328-1333.

[3] K. Micskei, L. Helm, E. Brücher, A. E. Merbach, *Inorg. Chem.* **1993**, 32, 3844-3850.

[4] H. G. Brittain, J. F. Desreux, *Inorg. Chem*. **1984**, 23, 4459-4466.

[5] G. Gonzalez, H. D. Powell, V. Tissières, A. E. Merbach, *J. Phys. Chem.* **1994**, 98, 53-59.

[6] Z. Luz, S. Meiboom, *J. Chem. Phys.* **1964**, 40, 2686-2692.

[7] F. A. Dunand, A. Borel, A. E. Merbach, *J. Am. Chem. Soc.* **2002,** 124, 710-716.

[8] J. H. Freed, *J. Chem. Phys*. **1978**, 68, 4034-4037.

[9] S. H. Koenig, R. D. Brown III, *Prog. Nucl. Magn Reson. Spectrosc.* **1991**, 22, 487-567.